Modeling a Coupled Machine-Inverter System

Final Project, EE290O: 21st Century Power System Dynamics

Anna Brockway[1,2], Ricky Liou[1], and Samantha Coday[1]

[1]Department of Electrical Engineering and Computer Sciences, [2]Energy and Resources Group

University of California, Berkeley

May 2019

I. Lin paper summary

A. Motivation

The increasing deployment of renewable energy prompts the need for a thorough analysis of how inverter-based energy generation sources will work with the current electricity system, which has been built around synchronous machines. Simulating the dynamics of the machine/inverter interface via modeling tools can help improve our understanding of the potential impacts of renewables deployment on grid operations and stability. Researchers from the National Renewable Energy Laboratory and the University of Minnesota sought to characterize the small-signal stability of such a coupled system [1]. Their work (here, "The Lin paper"), forms the basis for our modeling exercise this semester.

B. Approach

To model the machine/inverter interface, the researchers set up a framework consisting of a scalable three-phase inverter model, a synchronous machine model, and a load connected at a single point of common coupling (Fig. 1).

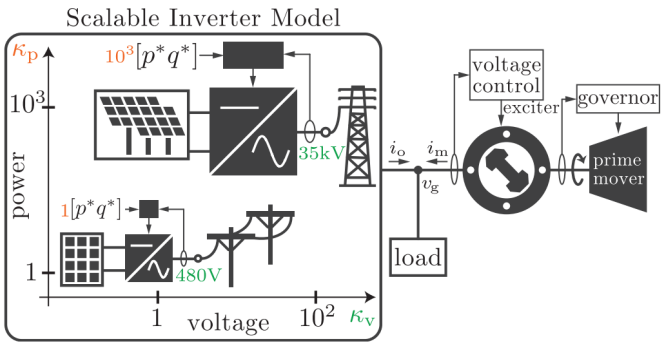

Fig. 1: Model of a single-machine single-inverter system, where the power and voltage ratings of the inverter are scalable. This model is an abstraction of low-inertia systems and is intended to assess possibly unforeseen dynamic interactions between machines and inverters as more inverters are installed in networks.

Fig. 1: The first figure from [1] is reproduced here with its caption. This figure shows the overall modeling setup used in this paper. The inverter model, shown producing current i_o, is on the left, the machine model, shown producing current i_m, on the right.

In this system, the synchronous machine sets the grid voltage, current, and frequency. The grid-following inverter produces current and matches the voltage of the machine. The current produced by the inverter and the synchronous generator are sent to the load.

1) Machine model: The machine model presented in the paper is meant to represent a "prototypical steam-driven generator" with a synchronous machine, exciter, governor, and prime mover (Figure 2, Table I). Separate frequency and voltage loops account for the machine rotor dynamics and electromagnetics, respectively [1]. The internal equations within each loop are presented in the Laplace domain, while the rest of the modeling in the paper occurs in the time domain. The model is not discussed in detail in the paper but readers are referred to [2] for reference.

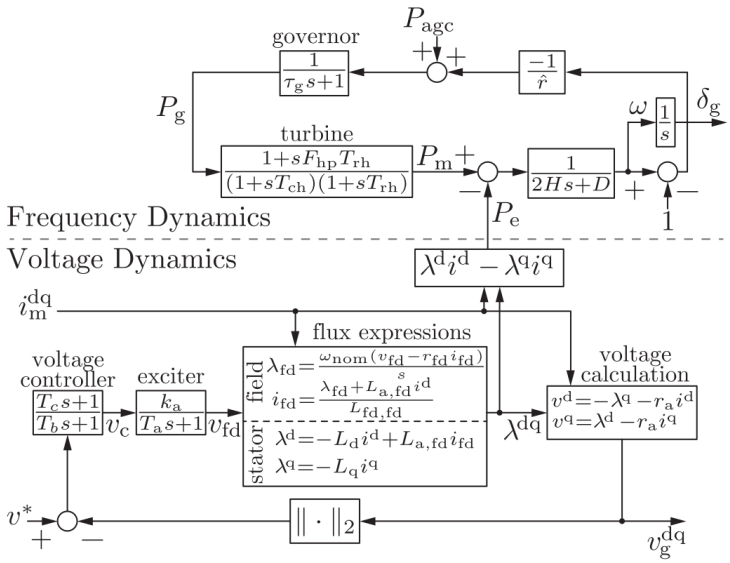

Fig. 2: Block diagram of a synchronous machine equipped with a prime mover, governor, and voltage excitation system.

Fig. 2: The machine model used in the Lin paper, reproduced from [1] with its caption. The model equations within the frequency and voltage loops are shown in the Laplace domain.

(a) Frequency Loop

Parameter	Value	Unit	Notes/Location used
H	2.9	s	inertia constant
D	1	p.u.	damping coefficient
$\hat{r}$	0.05	p.u.	armature resistance
τ_g	0.2	s	governor
F_{hp}	0.3	p.u.	turbine
T_{rh}	7	s	turbine
T_{ch}	0.3	s	turbine
P_{agc}	0.9	p.u.	AGC ref. signal (input)

(b) Voltage Loop

Parameter	Value	Unit	Notes/Location used
k_a	0.0745	p.u.	exciter
T_a	0.04	s	exciter
T_b	12	s	voltage controller
T_c	1	s	voltage controller
R_{fd} or r_{fd}	0.0006	p.u.	flux expressions
R_a or r_a	0.003	p.u.	voltage calculation
$L_{a,fd}$	1.66	p.u.	flux expressions
$L_{fd,fd}$	1.825	p.u.	flux expressions
L_d	1.81	p.u.	flux expressions
L_q	1.76	p.u.	flux expressions

TABLE I: Machine model parameters reproduced from [1] with notes. Two parameter names are provided where the same variable is referred to by different names in the text.

The state-space model is written as the following, with state variables and inputs collected in Table II:

$$\dot{x}_m = f_m(x_m, u_m) \tag{1}$$

$$x_m = [\delta_g, \omega, P_g, P_{gt}, P_m, v_c, v_{fd}, \lambda_{fd}]^T \tag{2}$$

$$u_m = [P_{agc}, v^*, i_m^{dq}]^T \tag{3}$$

(a) State Variables

Var.	Notes
δ_g	rotor angle that establishes dq reference frame
ω	frequency
P_g	governor output
P_{gt}	internal steam turbine state
P_m	mechanical power on the rotor
v_c	voltage controller output
v_{fd}	field voltage
λ_{fd}	field flux linkage

(b) Inputs

Variable	Notes
P_{agc}	AGC reference signal
v^*	terminal voltage command
$i_m^{dq} = [i_m^d, i_m^q]^T$	machine terminal currents

TABLE II: Machine model state variables and inputs, reproduced from [1].

The output of the machine model is the current i_m which is fed to the point of common coupling with the inverter model and the load.

2) Inverter model: The scalable power electronic inverter model used in the Lin paper is shown in Figure 3 with parameters listed in Table III. The inverter is designed to be "scalable" to enable the analysis of continuous power ratings and therefore the impact of "varying ratios of machine-to-inverter power ratings" [1]. The authors identify this built-in scaling flexibility as the "main contribution of our work" because it "addresses a critical challenge in modeling inverter-machine interactions: the large disparity in ratings between inverters and machines" [1]. Further, the authors claim that implementing this dynamical scaling approach enables them to investigate the impact of two

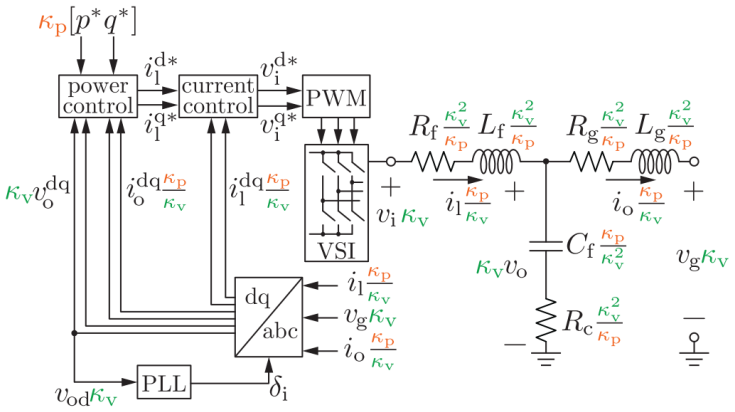

Fig. 3: Scalable three-phase inverter model with grid-following control. The power and voltage scaling factors are κ_p and κ_v respectively.

Fig. 3: The scalable grid-following inverter model used in the Lin paper, reproduced from [1] with its caption. This inverter model outputs current i_o, as labeled in Figure 1.

(a) Phase-Locked-Loop

Parameter	Value	Unit	Notes
k^p_{PLL}	0.25	rad/V	proportional-integral
k^i_{PLL}	2	rad/(Vs)	control gains

(b) Power Controller

Parameter	Value	Unit	Notes
k^p_{PQ}	0.01	1/V	proportional gain
k^i_{PQ}	0.1	1/(Vs)	integral gain

(c) Current Controller

Parameter	Value	Unit	Notes
k^p_i	16.4	V/A	compensator gains
k^i_i	30.4	V/(As)	

(d) LCL Filter

Parameter	Value	Unit	Notes
L_f	1e-3	H	1st branch inductance
R_f	0.7	ohm	1st branch resistance
L_g or L_o	0.2e-3	H	2nd branch inductance
R_g or R_o	0.12	ohm	2nd branch resistance
R_c	0.02	ohm	capacitor branch resistance
c or C_f	24e-6	F	capacitance

(e) System and Scaling Parameters

Parameter	Value	Notes
P_i	1 kW	unscaled inverter power rating
V_i	120 V_{LN}	line-to-neutral voltage rating
$\bar{P}_i$	$= \kappa_p P_i$	scaled inverter power rating
$\bar{V}_i$	$= \kappa_v V_i$	scaled voltage rating
κ_p	$\kappa_p p^* = \bar{P}_i$ when $\bar{P}_i < 250MW$	
	$\kappa_p p^* = 250MW$ when $\bar{P}_i > 250MW$	
κ_v	$\frac{24e3}{\sqrt{3}\times 120}$	compatible with machine

TABLE III: Inverter model parameters reproduced from [1] with notes. Two parameter names are provided where the same variable is referred to by different names in the text.

scenarios: "i) connecting many small inverters in parallel to obtain a larger aggregate, or ii) designing an inverter with a higher power level from some known nominal specifications" at "varying levels of inverter penetration" while preserving the ability to glean insights from the elemental one-machine one-inverter one-load setup shown in Figure 1 [1].

The inverter model contains two physical components, the output LCL filter and three-leg voltage source inverter, and three closed-loop controllers: the phase-locked-loop (PLL), current controller, and power controller. The PLL measures the frequency and voltage of the grid and produces the angle for the dq transformation. The power controller produces a current reference, and the current controller produces a voltage that is then fed through the voltage source inverter. The LCL filter yields the terminal current i_o.

The state-space model is written as the following, with state variables and inputs collected in Table IV:

$$\dot{x}_i = f_i(x_i, u_i) \tag{4}$$

$$x_i = [i_1^{dq}, i_o^{dq}, v_o^{dq}, \gamma^{dq}, p_{avg}, q_{avg}, \phi_{pq}, v_{PLL}, \phi_{PLL}, \delta_i]^T \tag{5}$$

$$u_i = [p^*, q^*, v_g^{dq}]^T \tag{6}$$

(a) State Variables

Variable	Vector defn.	Unit	Notes	Component
i_1^{dq}	$= [i_1^d, i_1^q]^T$	A	filter current	LCL
i_o^{dq}	$= [i_o^d, i_o^q]^T$	A	terminal current	LCL
v_o^{dq}	$= [v_o^d, v_o^q]^T$	V	filter voltage	LCL
γ^{dq}	$= [\gamma^d, \gamma^q]^T$		states for current PI controller	controllers
p_{avg}		W	low-pass-filtered measurement of inverter real power	controllers
q_{avg}		VAR	low-pass-filtered measurement of inverter reactive power	controllers
ϕ_{pq}	$= [\phi_p, \phi_q]^T$		states for real and reactive power PI controllers	controllers
v_{PLL}		V	filtered d-axis voltage measurement	PLL
ϕ_{PLL}			PI compensator state for PLL	PLL
δ_i		rad	angle for dq transformation	PLL

(b) Inputs

Variable	Vector defn.	Unit	Notes
p^*		W	unscaled real power set point
q^*		VAR	unscaled reactive power set point
v_g^{dq}	$= [v_g^d, v_g^q]^T$	V	unscaled grid voltage at point of interconnection

TABLE IV: Inverter model state variables and inputs. Variable, vector definition, unit, and notes columns are reproduced from [1]. The component column indicates which component model was used to separately test the performance of this state variable.

3) Model combination and implementation: The machine and inverter models operate in two different dq reference frames. To combine the models, the authors perform a coordinate transformation to put the machine terminal variables in the inverter reference frame, which is defined by the PLL angle δ_i [1]. The final network variables are thus located in the inverter reference frame, and the coupled machine-inverter model is defined by:

$$V_g = z(I_m + I_i) \tag{7}$$

$$I_m = i_m^d + j i_m^q \tag{8}$$

$$I_i = i_o^d + j i_o^q \tag{9}$$

Where equation 7 describes the relationship between the grid voltage, the complex load impedance z, and the terminal machine and inverter currents, which are further defined by equations 8 and 9. The case study parameters for the system used to implement the stability analysis are located in Table V.

(a) System parameters (base values)

Var.	Value	Unit	Notes
$\bar{P}_m$	555	MVA	
	24	kV	line-to-line voltage rating
ω_{nom}	$2\pi \times 60$	rad/s	nominal system frequency

(b) Load impedance consumption at nom. voltage

Value	Unit
500	MW
50	MVAR

TABLE V: Case study parameters from [1].

C. Results

Once the full model is created, the authors modify inertia and control parameters of the machine and inverter components. Eigenvalue analysis of the linearized model then provides insight into small-signal stability under different system setup conditions. The results of the small-signal stability analysis are shown in Figure 4. The authors chose to study the stability impacts of "bypass[ing] and/or modify[ing] various subsystems within the inverter and machine models" at increasing levels of inverter penetration [1].

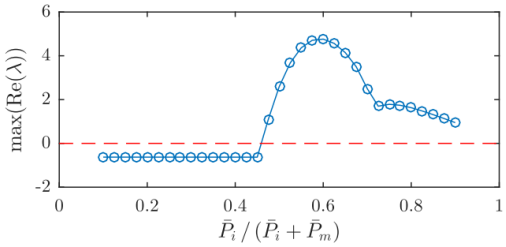

Fig. 4: Nominal case: Small-signal stability is ensured for penetration levels approaching 50%.

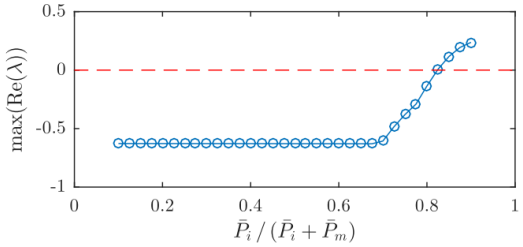

Fig. 7: Bypassing the PLL (assuming $\delta_{\mathrm{i}} = \delta_{\mathrm{m}}$) guarantees stability for penetration levels greater than 80%.

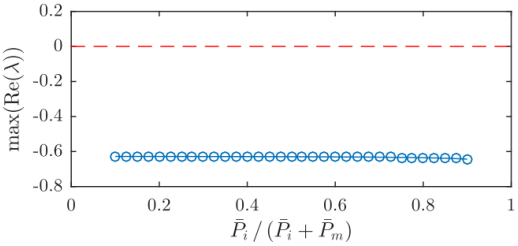

Fig. 5: Bypassing the machine AVR and exciter circuit significantly improves stability margins.

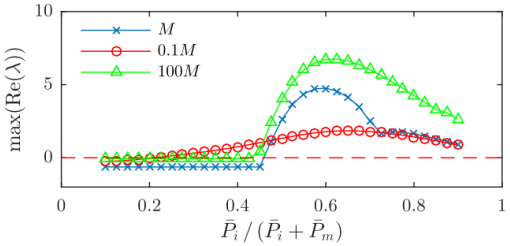

Fig. 8: System eigenvalues after modifying the machine rotor inertia.

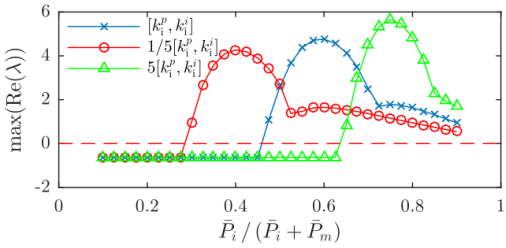

Fig. 6: Reduced current-controller gains adversely impact small-signal stability.

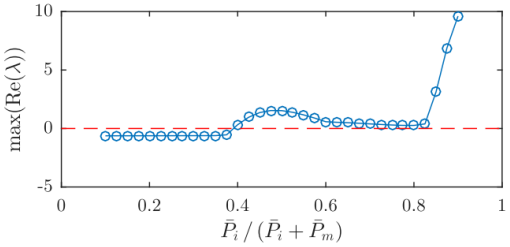

Fig. 9: Eigenvalues with the inverter power controller bypassed.

Fig. 4: Small-signal stability analysis results, reproduced with original captions from [1]. These are referenced in the present text by appending the original figure numbers.

In the nominal case, with all model components in place, the authors found that the system was stable for inverter penetration levels below approximately 50% (Figure 4.4). Next, the authors study the impacts of bypassing three components of their model (Figures 4.5, 4.7, and 4.9) and varying key parameters for two (Figures 4.6 and 4.8).

The system is stable for all penetration levels up to 100% when the machine exciter circuit and automatic voltage regulator (AVR) are removed from the system model (Figure 4.5). The authors suggest this may be due to interactions between the AVR and exciter circuitry, and that the specific components used may therefore play

a major role in the stability of coupled machine-inverter systems. The stability region is also increased when the authors bypass the PLL, instead assuming that the inverter has perfect knowledge of the grid frequency (Figure 4.7). This suggests that improving PLL performance may enhance the stability of coupled machine-inverter systems. However, when the inverter power controller is bypassed, the stability region does not change significantly (Figure 4.9).

Modifying the current controller gains from the baseline values has a significant impact on system stability, suggesting that "more aggressive current control gains increase the range of stable penetration levels" [1] (Figure 4.6). However, modifying the inertia of the machine rotor does not significantly impact the small-signal system stability (Figure 4.8).

D. Key assumptions

1) Machine Model Assumptions: In this work, it is assumed that the machine is connected to a perfectly balanced three phase system. It is also assumed that there is "perfect" knowledge of the machine parameters. The work details eighteen different machine parameters used in the model, all of which are assumed to be perfectly defined. There is no power system stabilizer included and no non-linear control elements.

2) Inverter Model Assumptions: Similar to the machine model, it is assumed that all parameters are known, and do not vary with operation. For example, the value of the capacitance does not change with frequency, temperature and bias the way a real capacitor would. It is also assumed that the model is an average model where switching dynamics are ignored. The largest assumption made in this work is the idea of a "scalable inverter." It is assumed that multiple inverters which are connected together can be modeled with scaled factors. The model ignores any effect produced from the interconnect of inverters.

3) Interconnect Assumptions: The model assumes a network with no real dynamics. The system is modeled with no series impedance and just a shunt load. This means that the voltage at the motor and inverter are equal.

4) Testing Assumptions: While analyzing small signal stability, each subsection was isolated by adjusting the model. For example, when testing the impact of PLL penetration the model is adjusted to assume the inverter has perfect alignment with the grid angle/frequency.

E. Merits

The main contributions of this work is the small signal stability analysis for each subsection of the model. As explained in Section I-C, the paper goes through each subsection of the system (i.e. PLL, current controller, machine AVR, etc.) and analyzes the stability dependent on different penetration levels. The authors conclude that the gains

of the inverter current controller have a large impact on the stability of the system. In addition, they find that the AVR has destabilizing interaction with the inverter current controller. This analysis shows which portions of the system need further investigation and careful design to ensure stability.

The ”scalable” inverter model is another significant merit of this work. By providing such a simple model to describe multiple inverter connections, the problem of power converter's interaction on the grid becomes greatly simplified. This allows for modeling and analysis of renewable penetration without having to take into consideration any effects that occur when connecting several inverters in parallel.

F. Shortcomings

While this work provides great insight into the stability analysis of advanced systems the shortcomings of this work are due to over-simplified assumptions. For example, the lack of dynamics in the line connecting the inverter and machine neglects any real effects of power transfer. These dynamics are known to have importance, and therefore future work will need to investigate penetration with additional line dynamics.

II. Semester project objectives

A. Planned objectives

Our goals for the semester can be summarized with the following questions:

- Can we replicate the stability results found in the Lin work?
- Does the stability remain the same if line dynamics are added?
- If the parameters of the machine and inverter are not known exactly how is the stability effected? (i.e. How does parameter sensitivity effect stability?)

B. In practice

The complexity of the work was greater than anticipated, so instead our final goals can be summarized as below.

- Can a simplified machine model and the inverter model described in the Lin work be replicated and understood?
- How does parameter sensitivity affect the model?

III. Detailed model description

A. Inverter model

1) PLL: The first part of the inverter model is the phase-locked-loop. The PLL dynamics are given by:

$$\dot{v}_{PLL} = \omega_{c,PLL}(v_o^d - v_{PLL}) \tag{10}$$

$$\dot{\phi}_{PLL} = -v_{PLL} \tag{11}$$

$$\dot{\delta}_i = \omega_{nom} - k_{PLL}^p v_{PLL} + k_{PLL}^i \phi_{PLL} = \omega_{PLL} \tag{12}$$

where $\omega_{c,PLL}$ is the cutoff frequency for the low pass filter for the v_o^d measurement, ω_{nom} is the nominal ac frequency, and k_{PLL}^p, k_{PLL}^i are the gains for the PI controller. The PLL dynamics drive the error in the d coordinate to zero, meaning that the PLL aligns its q axis to the external voltage. For testing purposes we set the grid voltage to $2\pi \times 60 = 377$ radians and the cutoff frequency to 250 Hz.

For implementation, the PLL dynamics equations were followed directly from the Lin work as described above. The input to the PLL, v_o^d, was set as a cosine function $v_o^d = 24e3 \times \cos(\delta_g - \delta_i)$ to test the ability of the PLL to correctly track the angle.

2) LCL: The final part of the inverter model is the LCL filter that interfaces the inverter terminal voltage v_i and the grid voltage v_g (Figure 3). Equations governing the behavior of the LCL were not provided by the authors of the Lin paper, so we derived them ourselves.

In the time domain, the internal states of the filter are governed by the following differential equations:

$$\frac{di_1}{dt} = \frac{1}{L_f}(v_i - i_1 - v_o) \tag{13}$$

$$\frac{dv_c}{dt} = \frac{1}{C}(i_1 - i_o) \tag{14}$$

$$\frac{di_o}{dt} = \frac{1}{L_g}(v_o - v_g - i_o R_g) \tag{15}$$

$$v_o = (i_1 - i_o)R_c + v_c \tag{16}$$

where the additional variable v_c is the voltage across the capacitor (Figure 5). We assume that the quantities are one phase of a balanced three phase system and so can be represented in the α, β domain. The following relationship is used to convert the quantities into a rotating frame:

$$\frac{d}{dt}x^{dq} = \frac{dx^{\alpha,\beta}}{dt} - e^{J\pi/2}\omega_s x^{dq} \tag{17}$$

where ω_s is the rotating frame's frequency and $e^{J\theta}$ is the rotation matrix by θ. Using the above equation, the

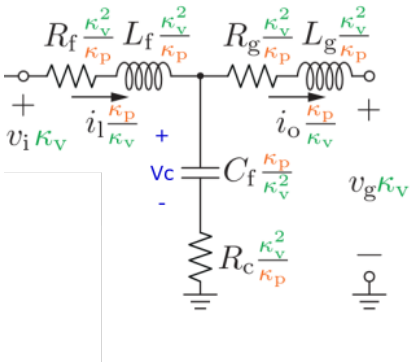

Fig. 5: LCL filter with capacitor voltage labeled in blue.

dynamics of the state variables in the dq domain are:

$$\frac{di_1^{dq}}{dt} = -e^{J\pi/2}\omega_s i_1^{dq} + \frac{1}{L_f}\left(v_i^{dq} - i_1^{dq} - v_o^{dq}\right) \tag{18}$$

$$\frac{dv_c^{dq}}{dt} = -e^{J\pi/2}\omega_s v_c^{dq} + \frac{1}{C}\left(i_1^{dq} - i_o^{dq}\right) \tag{19}$$

$$\frac{di_o^{dq}}{dt} = -e^{J\pi/2}\omega_s i_o^{dq} + \frac{1}{L_g}\left(v_o^{dq} - v_g^{dq} - i_o^{dq} R_g\right) \tag{20}$$

$$v_o^{dq} = (i_1 - i_o)R_c + v_c^{dq} \tag{21}$$

The rotation matrix is defined as:

$$e^{J\theta} = \begin{bmatrix} cos(\theta) & -sin(\theta) \\ sin(\theta) & cos(\theta) \end{bmatrix} \tag{22}$$

For implementation, the LCL was modeled using the DQ equations explained above. In contrast to the Lin work, v_c^{dq} was used as a state variable instead of v_o^{dq}. This was done for simplicity since the capacitor dynamics are the important system to observe. The only difference between V_c and V_o is the voltage across the resistor R_c. R_c is nominally 20 mω so this voltage is relatively small. The v_o^{dq} was calculated internally for the feedback of the power and current controllers.

3) Power Controller: The real and reactive power of the inverter are:

$$p = \frac{3}{2}[v_o^{dq}]^T i_o^{dq} \tag{23}$$

$$q = \frac{3}{2}[v_o^{dq}]^T \begin{bmatrix} 0 & -1 \\ 1 & 0 \end{bmatrix} i_o^{dq} \tag{24}$$

The dynamics in the power controller are given by:

$$\dot{s}_{avg} = \omega_c \left([p, q]^T - s_{avg} \right) \tag{25}$$

$$\dot{\phi}_{pq} = [p^*, q^*]^T - s_{avg} \tag{26}$$

where $s_{avg} = [p_{avg}, q_{avg}]^T$, w_c is the cutoff frequency for the low pass filter for s_{avg}, and p^*, q^* are the reference real and reactive powers. For testing purposes we set the cutoff frequency to be 250 Hz, which is the same value used as the cutoff in the PLL.

Current commands are derived from the the above states:

$$i_1^{dq*} = k_{PQ}^p \dot{\phi}_{pq} + k_{PQ}^i \phi_{pq} \tag{27}$$

where k_{PQ}^p is the proportional gain of the power controller and k_{PQ}^i is the integral gain of the power controller.

4) Current Controller: The current controller error is defined by Eqn. 28.

$$\dot{\gamma^{dq}} = i_1^{dq*} - i_1^{dq} \tag{28}$$

This error term is then used to determine the switch terminal voltage as seen in Eqn. 29.

$$v_i^{dq*} = k_i^p \dot{\gamma^{dq}} + k_i^i \gamma^{dq} + \begin{bmatrix} 0 & -1 \\ 1 & 0 \end{bmatrix} \omega_{PLL} L_f i_1^{dq} \tag{29}$$

where k_i^p is the proportional gain of the current controller and k_i^i is the integral gain of the current controller. However, through testing we found that Eqn. 29 was incorrect. We found instead that Eqn. 29 should have an additional term for v_o (shown in Eqn. 30). It is unclear why the original equation was missing this v_o term as it is necessary for finding the voltage at the switch terminal.

$$v_i^{dq*} = k_i^p \dot{\gamma^{dq}} + k_i^i \gamma^{dq} + \begin{bmatrix} 0 & -1 \\ 1 & 0 \end{bmatrix} \omega_{PLL} L_f i_1^{dq} + v_o \tag{30}$$

It also can be noted that both Eqn. 29 and Eqn. 30 do not include the voltage drop across the resistance in parallel with the L_f. While it is assumed this was discounted since it is a small voltage drop, the accuracy of the system could be increased with the addition of this voltage.

B. Machine model

We chose to focus on the inverter model and avoid the Laplace implementation of the machine model. Instead, we implemented a simple two-state model, as described in [3] (section 15.1).

$$\frac{d\delta_m}{dt} = \omega_{nom} \times (\omega_m - \omega_g) \tag{31}$$

$$\frac{d\omega_m}{dt} = \frac{1}{2H}(p_m - p_e - D(\omega_m - \omega_g)) \tag{32}$$

$$p_e = \frac{v_m \times v_g}{X} \times \sin(\delta_m - \theta_g) \tag{33}$$

The two-state model consists of two mechanical differential equations (31, 32) and a power transfer equation (33). This classical model neglects the electro-magnetic dynamics of the machine.

IV. Computing process

A. Model structure

We tested each component of the inverter model separately in Matlab using the ode15s solver. We used ode15s, as discussed in class, because it is well-suited to solve stiff differential equations. Each component model was run as a function from a main script.

We started by seperately testing and validating the PLL model while it was connected to an infinite bus. We then tested and validated the LCL model also via an infinite bus. We added the current controller to the LCL model without the power controller by assuming a static current reference. We then attempted to add the power controller. The machine model was formulated as a separate Matlab function and also tested with the ode15s solver.

B. Initial conditions

1) Inverter model: Setting meaningful and self-consistent initial conditions is a non-trivial task. Initial conditions are found based off a solution to a system of equations. Three criterion include initializing into an equilibrium point, satisfying Kirchoff's voltage and current laws, and achieving a desired power flow. Initializing into an equilibrium point means that the equations 18 - 20 must be equal to zero. The MATLAB function fsolve proved to be very useful in solving for the equilibrium points. To prove that the controllers and the system components were working, we set some states slightly differing from those values and observed if the states converged to the equilibrium point.

We back calculated the proper initial values for the integrator states so that the variables would start off at the proper values. In our current controller $i_1^{dq*} = k_{PQ}^p \dot{\phi}_{pq} + k_{PQ}^i \phi_{pq}$. We set the initial condition of ϕ_{pq} so that $k_{PQ}^i \phi pq$ equaled our desired reference current. Similarly, the integral term in the power controller had to be initialized.

The initial conditions for the inverter states were calculated with the aid of phasor diagrams as seen in Figure 6. The angles between each phasor were chosen to be $30°$. The current phasor bisects the voltages V_g, V_o, V_i because

it is assumed that the effect of the resistances is little and also that the magnitudes of each voltage are the same. The voltages have the shown phase relationship (V_i leading V_o leading V_g) in order to have positive power flowing from the inverter into the grid.

The grid voltage was set to $[0, 24kV]$. Because the angle and magnitude of V_o is set, it can be calculated by rotating V_g by 60° using the rotation matrix in (22). The current I_o is found through:

$$I_o = \frac{V_g - V_o}{j\omega_s L_g} \tag{34}$$

The remaining values V_i and I_1 are found in the same exact way.

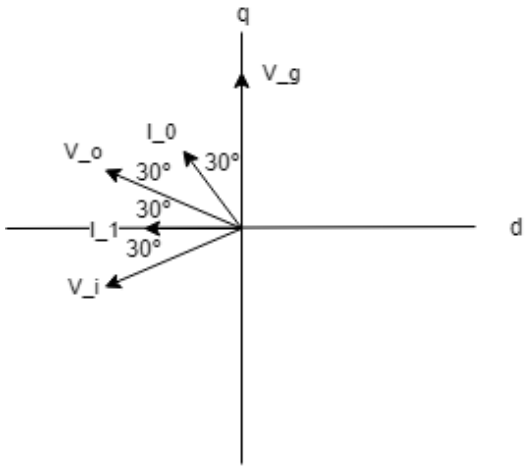

Fig. 6: Phasor diagram of initial conditions in inverter

State variable	Unit	Initial condition	Description	Component
$i_1^{dq} = [i_1^d, i_1^q]^T$	A	[-24e3, 0]	filter current	LCL
$i_o^{dq} = [i_o^d, i_o^q]^T$	A	[-12.03e3, 20.83e3]	terminal current	LCL
$v_c^{dq} = [v_c^d, v_c^q]^T$	V	[-20.78e3, 12e3]	capacitor voltage	LCL
$\gamma^{dq} = [\gamma^d, \gamma^q]^T$		[0, -395]	states for current PI controller	controllers
p_{avg}	W	500e6	low-pass-filtered measurement of inverter real power	controllers
q_{avg}	VAR	50e6	low-pass-filtered measurement of inverter reactive power	controllers
$\phi_{pq} = [\phi_p, \phi_q]^T$		[-240e3, 0]	states for real and reactive power PI controllers	controllers
v_{PLL}	V	0	filtered d-axis voltage measurement	PLL
ϕ_{PLL}		0	PI compensator state for PLL	PLL
δ_i	rad	0	angle for dq transformation	PLL
δ_g	rad	$2\pi/3$	grid angle	PLL

TABLE VI: Initial conditions for inverter state variables.

2) Machine model: The classical machine model has three states that are all per-unitized. We set the initial conditions for the machine rotor angle (δ_m), machine frequency (ω_m), and machine power (p_e) to 0, 1, and 1, respectively (Table VII). These initial conditions are consistent with a machine model that matches the grid frequency, outputs its full power rating, and stabilizes at a small rotor angle for ideal power transfer.

State variable	Unit	Initial condition	Description
δ_m	p.u.	0	rotor angle
ω_m	p.u.	1	frequency
p_e	p.u.	1	power

TABLE VII: Initial conditions for machine state variables.

The two mechanical differential equations (31, 32) used in the machine model can be initialized as normal states. However, the power transfer function (eq.33) is an algebraic constraint. Initializing this variable required: re-writing its full equation to be equal to zero, including that equation as a returned state variable, and using a diagonal 3-by-3 mass matrix via ordinary differential equation options to set the equation to zero in Matlab.

V. Modeling Results

A. Inverter model

1) PLL: Figure 7 shows the PLL syncing with a grid voltage. Shown in the figure is the angle of the grid compared to that of the d axis inside the PLL, where the angle is defined with respect to stationary α, β axes. The first row of the figure depicts the PLL state variables. The filtered d-axis voltage measurement is driven to zero so that the q axis is aligned with the external voltage. The PI compensator gain is whatever it needs to be to drive the

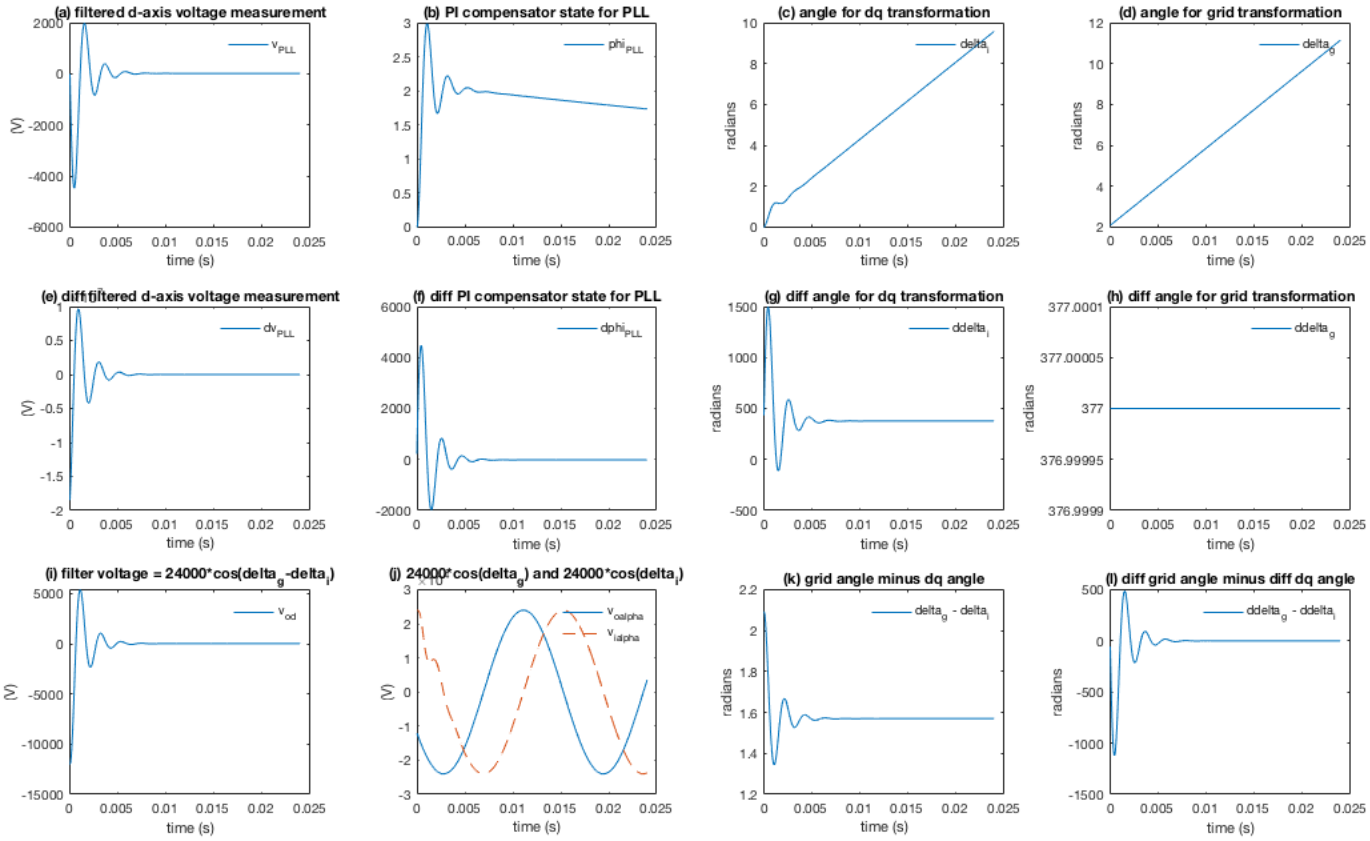

Fig. 7: PLL Operation

DC error to zero. The derivatives of the states are seen in the second row. The d-axis voltage and PI compensator states are virtually not changing, so their derivatives are zero. The angular frequency of the dq axis settles at the synchronous frequency of 377 rad/s. The third row shows that the dq axes and the external grid voltage settle to a 90° offset, as the grid voltage is aligned with the q axis when the PLL is properly synced.

2) LCL: Figure 8 shows the simulation results when the LCL filter was isolated and run independently of the system. An infinite bus was connected to the output of the LCL filter for testing purposes. Figure 8 shows that all state variable come to steady state quickly and the steady state values are supported by KCL and KVL analysis of the filter.

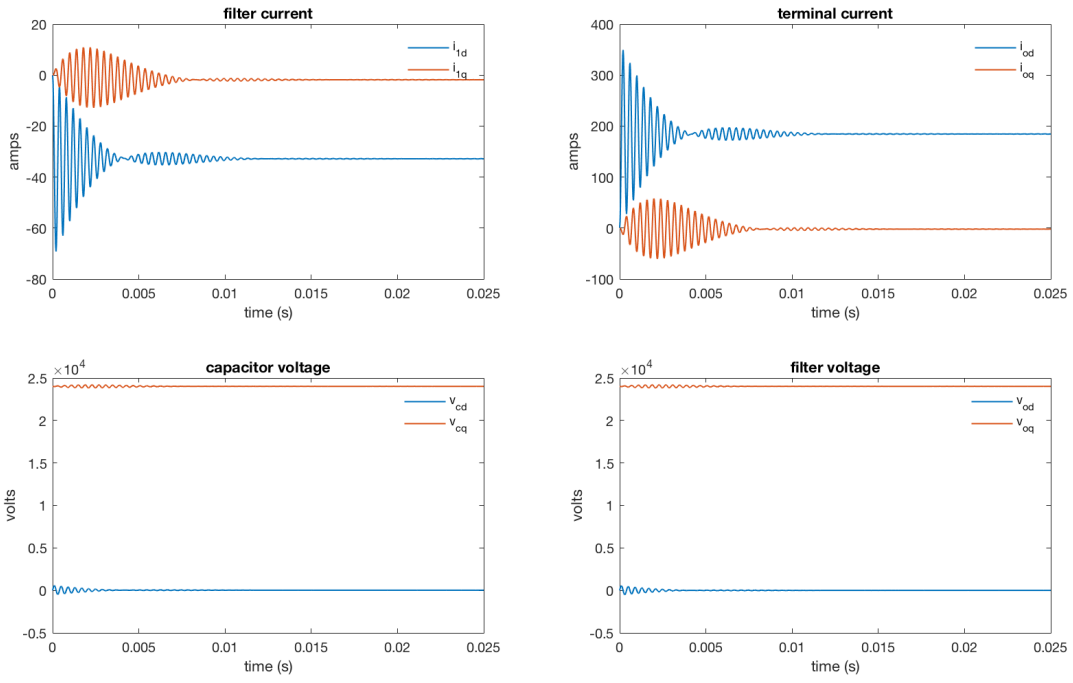

Fig. 8: LCL operation, $R_c = 0.02$.

Results in Figure 8 were collected when the R_C, seen in Figure 3, as the resistance in series with the capacitance, was set to 0.02 Ω which was the value given in the Lin work. In [4] a detailed derivation of LCL stability is performed and it is found that the value of the capacitance series resistance greatly effects the LCL stability. To confirm the results from [4] the R_c was increased to 2 Ω and the same simulation was performed. These results of the LCL can be seen in Figure 9. These results show that the system comes to steady-state in approximately one-tenth the time that the system in Figure 8 takes to come to steady state. It should be noted that the state-variables shown still have the same steady state values independent of the R_c value chosen. However, there is an optimum R_c for each system, because the larger the value, the more power dissipated, which is problematic in large current systems.

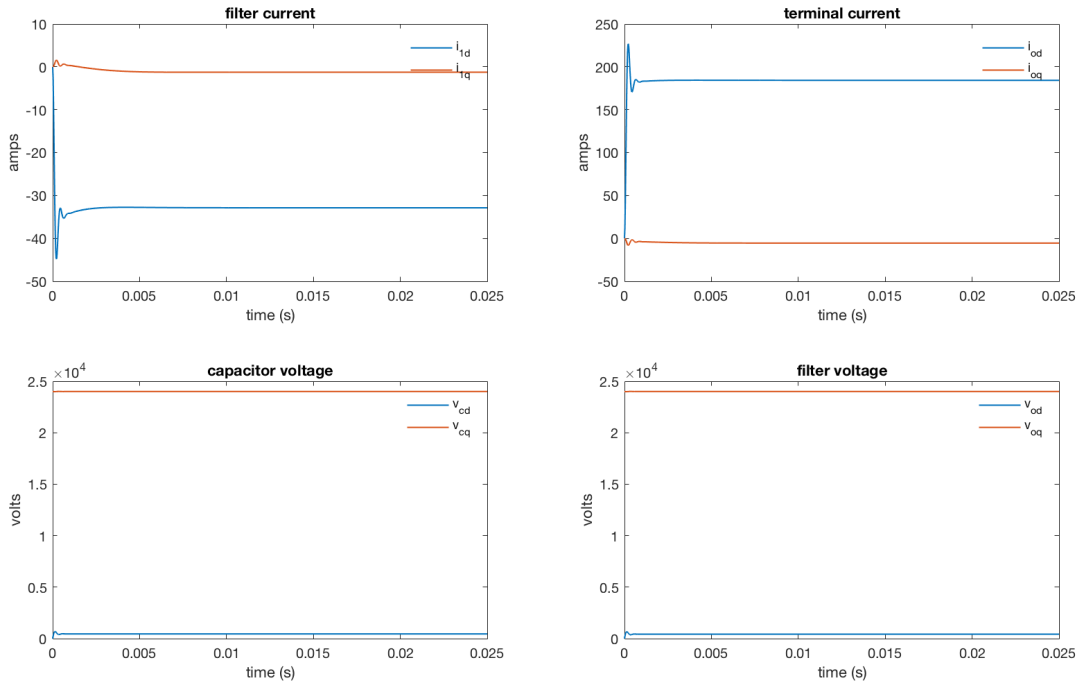

Fig. 9: LCL operation, $R_c = 2$.

3) LCL and current controller: Once the LCL performance was verified, the current controller was added. To test the performance of the current controller and LCL filter together, the current, i_1^{dq*}, was fixed. This eliminated the influence of the power controller. Figure 10 shows the currents and voltages of the LCL filter once the current

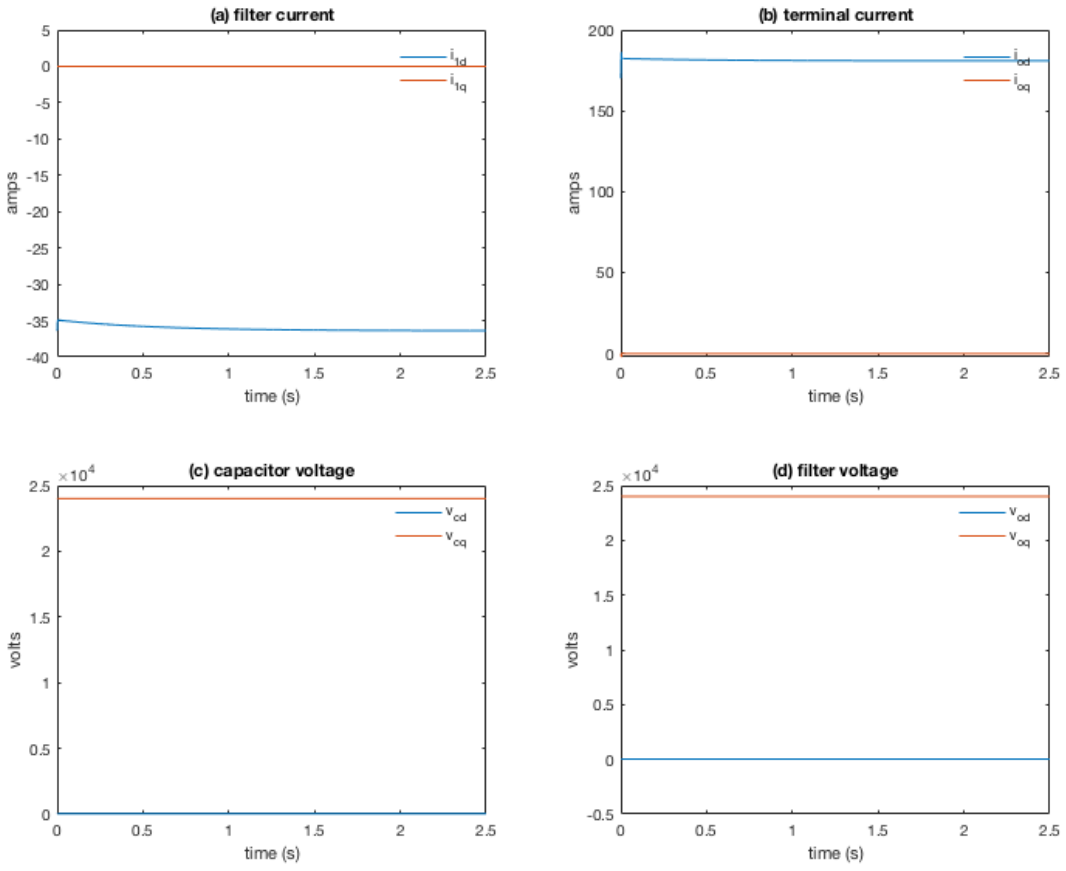

Fig. 10: Stability observed in currents and voltages when the current controller is added to the LCL controller.

controller was included. The i_1^{dq*} was fixed to [0, -36.4] A for these results, and it can be seen at steady state that i_1^{dq} is driven to the same value, which is the purpose of the current controller; to minimize the error between i_1^{dq} and i_1^{dq*}.

To verify the current controller performance under different operating conditions, the i_1^{dq*} was adjusted to [0, -40] A and the results can be seen in Figure 11. In the bottom two sets of figures, (b), it can be seen that i_1^{dq} is driven to the same value again. This validates the performance of the current controller and LCL filter.

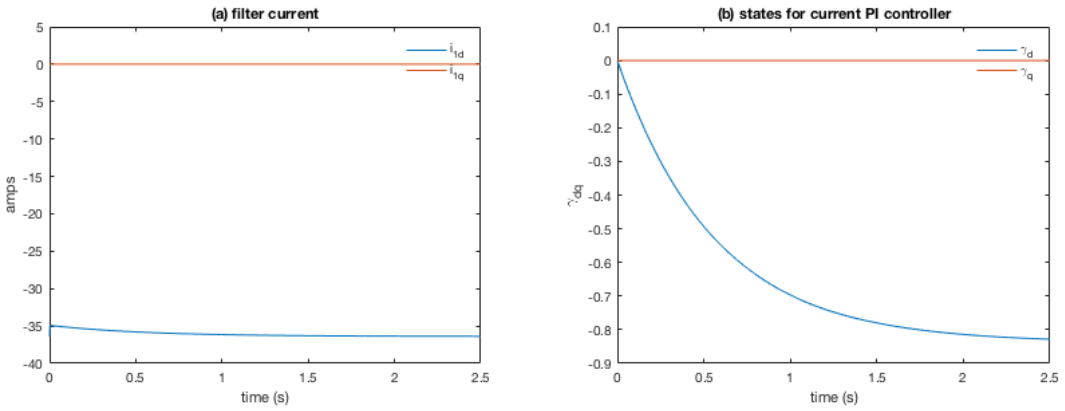

(a) $i_1^d = 0, i_1^q = -36.4$

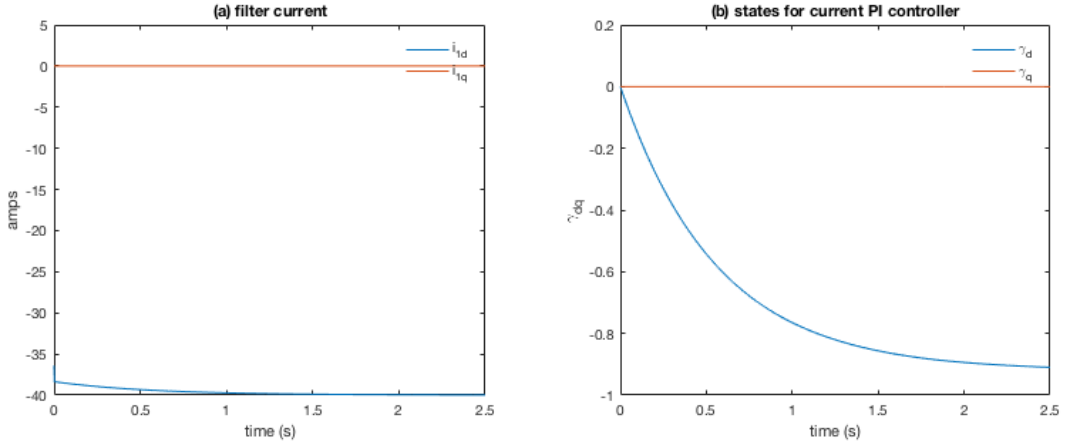

(b) $i_1^d = 0, i_1^q = -40$

Fig. 11: Filter current and current states for two desired convergence conditions on the LCL and current controller.

Figure 11 also shows the states of the PI controller. It is expected that at steady-state the derivative of the states, which represents the error should be zero. This is validated in Figure 11.

4) LCL, current, and power controller: Once the LCL and current controller performance was verified, the next step was to include the power controller. To test these three subsections together, the PLL was bypassed, by assuming perfect knowledge of the angle of the grid. The initial conditions were implemented as discussed in Section IV-B1. Unfortunately, the system was not able to reach stability, even after extensive troubleshooting. The instability of the system can be seen in Figure 12. While adjusting the gains of the PI controller, slowed down the time until instability, it did not create a stable system. Figure 12 shows that the negative feedback of the controller

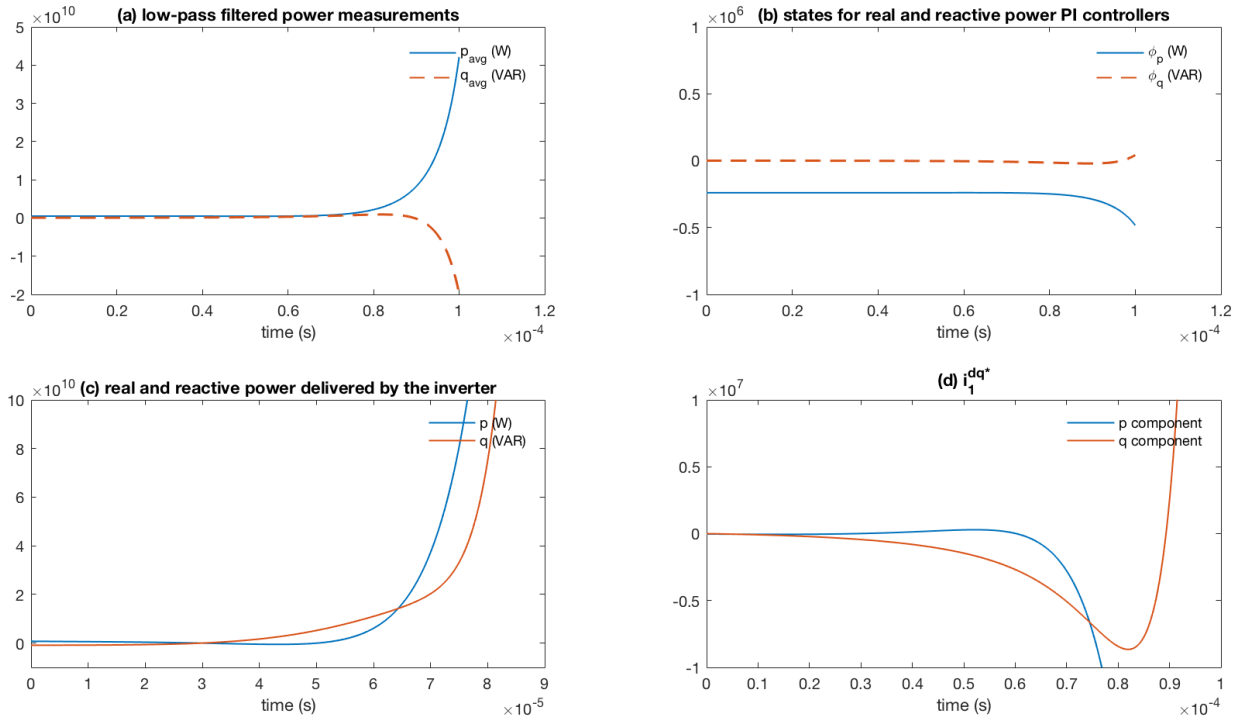

Fig. 12: Instability observed in power, state, and current measurements when the power controller is added to the LCL and current controller.

is unsuccessful, as the power and current delivered by the inverter reach unstable limits relatively quickly, even thought the initial conditions were set so the system would be close to stability initially.

Figure 13 further shows the instability, by showing the current controller is no longer stable with the addition of the power controller. The states of the current controller increase very rapidly which implies the error is increasing as well.

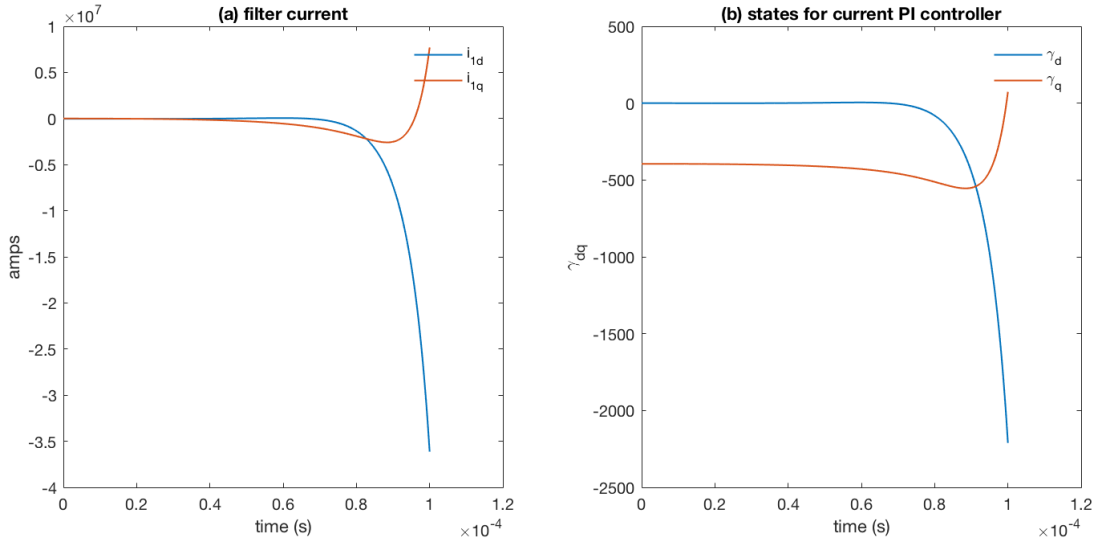

Fig. 13: Instability observed in current and state measurements when power controller is added to the LCL and current controller.

B. Machine model

Beyond the initial conditions, the other tunable parameters in our two-state machine model are the inertia constant (H), damping coefficient (D), and impedance (X) (equations 31, 32, 33). We began by setting these values to the respective terms described in the original machine model used by the authors of the Lin paper: H was set to 2.9 seconds, D to 1 p.u., and X to the value of the internal machine armature resistance r̂, 0.05 p.u. (Table I). These parameter choices resulted in an unstable machine model (Figure 14a). Increasing the damping coefficient by a factor of 10 to damp the instability reduced the oscillation of the state variables but did not lead to full convergence (Figure 14b). Our initial choice for the impedance, X, accounted just for the armature resistance. However, in the original power electronics equations, this term is meant to account for line impedance. Increasing X by a factor of ten gave us stable behavior (Figure 15). In our final two-state machine model, the machine frequency and power stabilize at 1 p.u. and the rotor angle stabilizes at 0.1674 p.u.

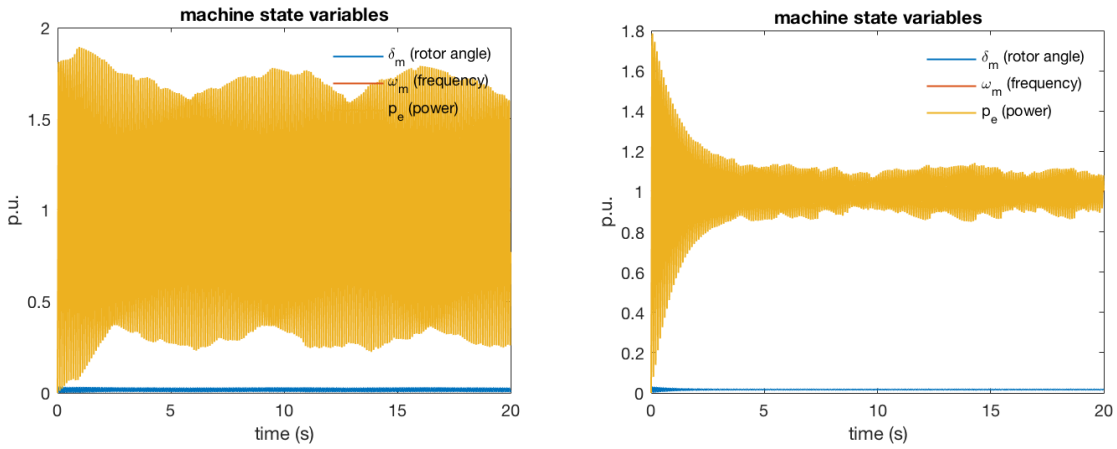

(a) D = 1, X = 0.05

(b) D = 10, X = 0.05

Fig. 14: Machine model implementation with changing parameters.

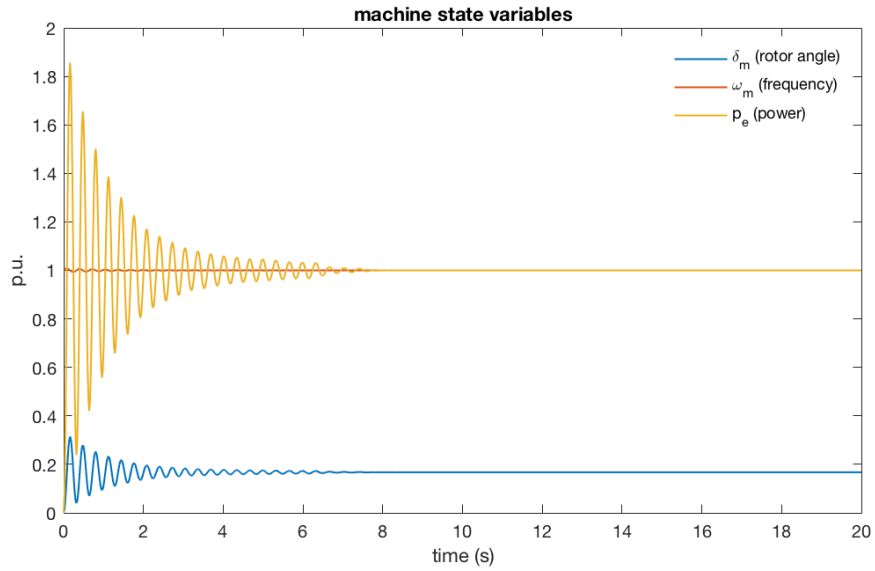

Fig. 15: Final machine model implementation (D = 10, X = 0.5).

VI. Lessons learned

A. Breaking apart the problem

We began with the inverter model and attempted to program the entire model at once. This method was unsuccessful, and we quickly realized it was important to test each subsection of the system building up the inverter model. By understanding how each subsection worked and troubleshooting at a smaller scale we were able to build the system up more effectively.

B. Initial Conditions

We found that the simulation models are extremely sensitive to initial conditions. Most of the time, the hours we spent debugging resulted in finding out that our initial conditions were not close enough to the equilibrium point. The MATLAB function fsolve was useful to find initial conditions. However, it did not always work well. Sometimes the solutions yielded by fsolve were actually unstable equilibrium points. When we input the results of fsolve directly into our model, the states did not change as expected. When we perturbed one state by an extremely small amount, the simulation would fail. Sometimes using fsolve would allow us to verify if the equations in our model were implemented correctly. If our model was not correct, the fsolve would fail or yield unstable equilibrium points.

Many times, choosing a proper initial condition was difficult due to the many degrees of freedom. It was difficult to determine which voltages / currents to fix and which should be a function of the others. Often times, starting off by picking the voltage / currents in the wrong order would force operating points far away from what we intended.

It was first thought that the integrator states should set to be zero to indicate that there was no past error. This proved to be incorrect. At equilibrium, the change of the integrator states is zero, but the integrator state itself is not necessarily zero. The value of the integrator is whatever it must be to set the DC error to zero. In the initialization process, we had to back calculate the proper initial values for the integrator states so that the variables would start off at the proper values. For example, in our current controller $i_1^{dq*} = k_{PQ}^p \dot{\phi}_{pq} + k_{PQ}^i \phi_{pq}$. Our thoughts at the beginning were to set the state variable ϕ to zero. At $t = 0$, this resulted in $i_1^{dq*} = 0$, a value far away from what we wanted. This resulted in an unstable system.

VII. Team member contributions

From the beginning, we decided as a team to tackle this project together. Instead of breaking up the problem, we met all three of us and worked through every aspect together. While this took coordination of time, we feel that it best helped us work through the problems since we all came in with little knowledge about the subject. Another positive aspect of our approach is that all of us now understand all subsections of our model, because we

all worked through it together. We think this approach helped us all learn the most from this experience. We also all contributed equally to the write-up of the final report.

REFERENCES

[1] Y. Lin, B. Johnson, V. Gevorgian, V. Purba, and S. Dhople, "Stability assessment of a system comprising a single machine and inverter with scalable ratings," *2017 North American Power Symposium, NAPS 2017*, 2017.

[2] P. Kundur, *Power system stability and control*. McGraw-Hill, Inc., 1994.

[3] F. Milano, *Power System Modelling and Scripting*. Springer, 2010.

[4] M. Huang, J. Sun, Y. Peng, and X. Zha, "Optimized damping for LCL filters in three-phase voltage source inverters coupled by power grid," *Journal of Modern Power Systems and Clean Energy*, vol. 5, no. 4, pp. 642–651, 2017.